Materials Chemistry and Physics 142 (2013) 213–219

Contents lists available at SciVerse ScienceDirect

Materials Chemistry and Physics

journal homepage: www.elsevier.com/locate/matchemphys

Characterization of nano-crystalline Mg–Ni–Al hydrotalcite derived mixed oxides as hydrogen adsorbent

M. Abdus Salam*, Suriati Sufian, T. Murugesan

Chemical Engineering Department, Universiti Teknologi PETRONAS, Bandar Sri Iskandar, 31750 Tronoh, Perak, Malaysia

HIGHLIGHTS

- Nano-crystalline mixed oxides as adsorbent synthesized using conventional coprecipitation.
- Mg–Ni–Al reduced mixed oxides showed 3.9 wt% reversible H_2 adsorption capacity.
- Physical and Chemical adsorption of hydrogen catalyzed by nickel.
- SAED pattern showed the hydrogen adsorbed phases of reduced mixed oxides.
- Raman and FT-IR analysis ensured the hydrogen adsorbed phases.

ARTICLE INFO

Article history:
Received 18 February 2013
Received in revised form
21 May 2013
Accepted 7 July 2013

Keywords:
Nanostructures
Oxides
Precipitation
Adsorption
Microstructure
Raman spectroscopy

ABSTRACT

A promising energy storage material containing magnesium, nickel and aluminum metals has been synthesized using conventional coprecipitation method. The physio-chemical properties, morphology and microstructure of hydrotalcite based mixed oxides (MNAM) have been characterized using ICP-MS, XRD, BET, FESEM and TEM techniques. The characterizations revealed that the adsorbent are highly dispersed, poly crystalline, homogenously distributed and interactive. Temperature programmed techniques have been used to explore the sorption capacities of mixed oxides. Nano-crystalline mesoporous and interactive reduced mixed oxides exhibit a 3.9 wt% H_2 adsorption capacity at ambient conditions. Temperature programmed desorption study predicted a desorption capacity of 1.9 wt% H_2. Different hydrogen adsorbed phases of magnesium and nickel have been characterized using HRTEM, Raman and FT-IR techniques.

1. Introduction

Hydrogen is a potential clean fuel for the future due to its availability, zero emission with water being the only combustion product when burnt it with oxygen. Metal hydrides are potential hydrogen storage materials that can meet the demands of energy for on board vehicles and fuel cells. Light metal hydride cannot adsorb hydrogen at room temperature and ambient pressure. Different hydride system release hydrogen at different temperature and time. Due to the potential hydrogen density of MgH_2, many investigations has been focused on developing its properties to overcome the common shortcomings of the materials such as stability, formation of surface oxides, slow diffusion of hydrogen and slow dissociation. Hydrogen storage can be done through a chemical storage method like metal hydrides and chemical hydrides [1]. Magnesium has been explored in different ways due to its high gravimetric and volumetric hydrogen density and its availability [2]. Magnesium can form a structure (MgH_2) with 7.6 wt % hydrogen. Nickel catalyses hydrogen to dissociate and enhance the hydrogen uptake [3]. When hydrogen combines with Magnesium (Mg), it forms the inter-metallic compound, Mg_2Ni which also forms a hydrogen-rich complex hydride Mg_2NiH_4 [4]. Materials that are capable to adsorb reversible hydrogen at near ambient conditions can fulfill the requirement of the U.S. department of energy (DOE) [5,6]. Reversible chemisorption is a potential way to reach the goal together with physisorption [7]. Some materials exhibit high hydrogen storage capacities such as Alanates and metal hydrides but their practical use is limited due to their non-favorable thermodynamics and kinetics and their regeneration limitation.

Nano-crystalline particles enhance hydrogen storage and release kinetics [8] and often show different behavior compared to

* Corresponding author. Fax: +60 5 365 6176
E-mail address: salam.bcsir@gmail.com (M.A. Salam).

0254-0584/$ – see front matter © 2013 Elsevier B.V. All rights reserved.
http://dx.doi.org/10.1016/j.matchemphys.2013.07.008

bulk particles. Mixed oxides have recently emerged as promising candidates to be hydrogen gas adsorbents. Hydrotalcite derived mixed oxides have important features in forming highly dispersed metallic nano-particles upon reduction [9]. Hydrotalcite based mixed oxides have gained considerable attention in being designed as adsorbents due to their wide variety of chemical compositions [10] and their textural and surface morphology that can be tuned. The surface of the reduced mixed oxides is more reactive than the oxide with the gases and can form possible yields due its acid-base surface energy [11]. Mixed oxides formation leads to the modification of an electronic structure, the band gap, Fermi level position and transport properties etc. in the solid solution [12]. Hydrogen adsorption on reduced mixed oxides had already been reported on $CeM_{0.5}Ni_xO_y$ and Cu added Fe/Ce/Zr mixed oxides were investigated by Jalowiecki et al., and Kim et al., [13,14], through experimentation at high temperatures. In the gas phase, hydrogen readily attaches to other molecules or atoms.

In this investigation, hydrotalcite based mixed oxides have been characterized as hydrogen adsorbent. The sorption capacities of material have been studied at ambient conditions to observe it practical application.

2. Material and methods

2.1. Mixed oxides preparation

The Hydrotalcite derived mixed oxides containing magnesium, nickel and aluminum (MNAM) were synthesized by using the conventional coprecipitation method [9] from metal nitrate precursors and Na_2CO_3 as the precipitating agent. Three solutions, each containing appropriate quantities of the metal nitrate precursors of magnesium, nickel and aluminum were prepared. The mixed metal nitrate solution added drop wise into a 0.5 M sodium carbonate solution maintaining the temperature at 55 °C with a vigorous stirring to get the optimum precipitation of hydrotalcite. The pH was varied from 12.5 to 9. The resulting precipitates were washed several times to remove the excess Na^+ and NO_3^- ions then filtered and dried. The fresh dried materials were calcined at 650 °C for 2 h to convert the mixed oxides. The mixed oxides samples were designated by MNAM-xyz, respectively; MNAM stands for Mg–Ni–Al mixed oxides and xyz stands for the molar ratios of the Mg:Ni:Al samples.

2.2. Adsorbent characterization technique

ICP-MS (**Inductively coupled plasma mass spectrometry**), from Agilent 7500 series has been used to analyze the distribution of metals in mixed oxides. Mixed oxides phase identification and its crystallinity were analyzed by powder X-ray diffraction (XRD) technique using a Bruker D8 advanced diffractometer with Cu-K_α radiation. Diffraction patterns were recorded in the range of $2\theta = 3°–80°$ with a step size of 0.04° and a counting time per step of 10 s. Nitrogen gas adsorption-desorption isotherms of the samples were obtained using a Micromeritics ASAP 2020 Sorptometer. The total surface areas (S_{BET}) were calculated with the Brunauer–Emmet–Teller (BET) method. The surface morphology of the mixed oxides were studied by using a Field-emission scanning electron microscope (FESEM) from the CARL Zeiss Supra 55VP instrument equipped with the Oxford INCA 400 EDX microanalysis system. The characterization of microstructure of mixed oxides has been carried out using a CARL Zeiss LIBRA^R 200FE Transmission electron microscope with an acceleration voltage of 200 kV on ultrasonically dispersed samples in isopropanol.

The hydrogen adsorption in the mixed oxides at ambient conditions was measured using a micromeritics ASAP 2020C, chemical adsorption apparatus. A 20 mg sample was reduced by a 5% H_2 gas balanced with N_2 gas flowing at 20 ml min^{-1} and, with the heating rate of 10 °C min^{-1} up to 850 °C than cool down the temperature to 30 °C before hydrogen adsorption isotherm analysis at 30 °C and a pressure ranging from 0 to 760 mmHg. Purified hydrogen gas (99.999%) was introduced to a separate gas inlet of the adsorption unit in order to measure the hydrogen adsorption.

The hydrogen reduced (TPR) mixed oxides were cleaned by pure nitrogen gas and then cooled down to 30 °C. The TCD signal was brought back to the baseline by flowing nitrogen for 15 min. The samples were maintained at 30 °C under a flow of hydrogen to adsorb hydrogen using the same analysis method mentioned above. The H_2-TPD was performed up to the temperature of 500 °C with a ramp of temperature of 5 °C min^{-1} and under the flow of nitrogen 20 ml min^{-1}. A gas calibration for the 5% H_2 in N_2 (20 ml min^{-1}) was performed to determine the TCD signal response. TCD responses represent the different concentration of H_2. The quantification of the peak area to the volume data of H_2-TPD were performed using calibration factor and sample amounts (weight).

The Raman spectra of hydrogen adsorbed mixed oxides of MNAM 211 powder was analyzed by a HORIVBA Jobin Yvon, HR800 spectroscopy equipped with micro-raman set up and 'NGSLabspec' computer program. The recorded spectral range was 0–6000 cm^{-1} and scanned the spectrum several times. The focal length of laser beam was 800 mm and focused to surface of the hydrogen adsorbed mixed oxides so that the area allowed to focusing on different particles.

The FTIR spectra of hydrogen adsorbed mixed oxide of MNAM 211 were recorded using Perkin elmer spectrum one FTIR spectrometer with auto image microscope attachment in the frequency region of 100–5000 cm^{-1}. The sample was finely ground with KBr before making disk and put into the sample holder. The background spectrum of KBr was recorded before the analysis.

3. Results and discussion

3.1. Metal composition of adsorbents

The elemental chemical analysis using ICP-MS is summarized in Table 1 where the results are shown in metal weight percent. The adsorbent contains fewer amounts of aluminum and higher quantities of divalent metals species than it was supposed. Well crystalline magnesium hydrotalcite usually form in higher pH condition. The presence of less quantity of aluminum cations in the solid solution can be explained as the trivalent aluminum used as support might not be precipitated fully during synthesis and the synthesis in strong basic condition at pH 10 is another cause in where the partial solubility of aluminum ions as aluminate species. The higher content of nickel in Mg–Ni–Al compositional mixed oxides is due to the partial replacement of the aluminum by nickel cations, which often occur at high pH value [15].

Table 1
Elemental composition and textural properties of MNAM with different molar ratios and textural properties.

Adsorbent name	$M^{II})/M^{III}$ (EXPT)	Elemental composition			BET surface area (m^2 g^{-1})
		Mg	Ni	Al	
MNAM-031	3.19	–	87	12.52	110
MNAM-121	2.96	14.12	69.78	16.10	284
MNAM-211	3.09	32.89	47.98	19.10	325
MNAM-301	2.94	72.59	–	27.40	120

The solubility product of Al $(OH)_3$ ($Ks = 10^{-33}$) is much lower than that of $Mg(OH)_2$ ($Ks = 10^{-11}$) and $Ni(OH)_2$ ($K_S = 10^{-15}$) and a very high pH was required to co-precipitate Mg(II), Ni(II) and Al(III) hydroxides. At low pH even at pH 4.0, Al $(OH)_3$ starts to form and contaminate the hydrotalcite that forms at higher pH (above 8). At higher pH, aluminum ions form aluminate anions $[Al(OH)_4^-]$ that dissolve in the solution. As a result, no aluminum hydroxide precipitates and it does not show any contamination of the hydrotalcite with aluminum hydroxide. At high pH, magnesium hydroxides precipitated in which obtained hydrotalcite does not contaminate with magnesium hydroxides at this condition.

Binary mixed oxides of MNAM 031 displayed slightly higher amount of nickel compare to synthesis solution. This is due to the partial replacement of aluminum. At pH less than 10, magnesium precipitates less than it was supposed due to the non-favorable synthesis environment. The ratios of the metal in the mixed oxides are close to the value in the starting solutions (synthesis molar ratio). The results demonstrate that the degrees of the precipitation of the metals are about 95%, and the mixed oxides are homogenously distributed.

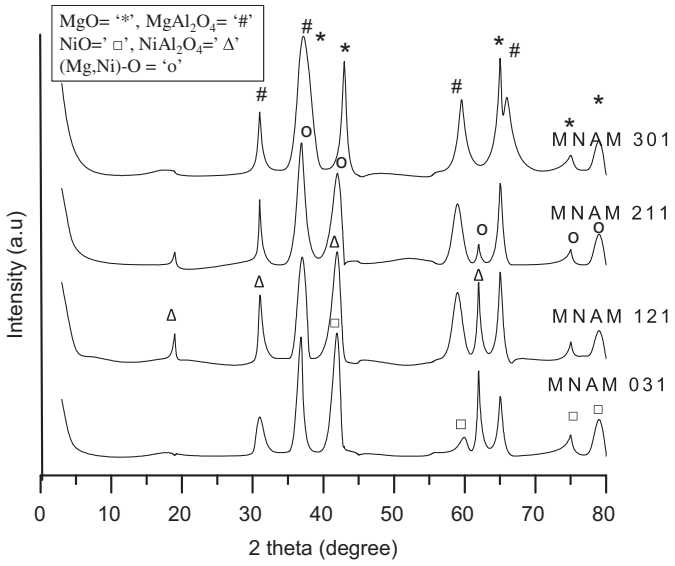

Fig. 1. XRD pattern of mixed oxides with different molar ratios.

3.2. Thermal decomposition and phases chracterization of adsorbents

Mg–Ni–Al hydrotalcite decomposition can be performed through a few steps such as dehydration, dehydroxylation and the decomposition of anions and resultant yields are the crystalline mixed oxides as shown by a typical equation below [16].

$$[Mg_{0.50}Ni_{0.25}Al_{0.25}(OH)_2] \times [(CO_3)_{0.13}]0.39\ H_2O \rightarrow [Mg_{0.50}Ni_{0.25}Al_{0.25}(OH)_2] \times [(CO_3)_{0.13}] \rightarrow [Mg_{0.50}Ni_{0.25}Al_{0.25}O_{1.13}] \times [(CO_3)_{0.13}] \rightarrow [Mg_{0.50}Ni_{0.25}Al_{0.25}O_{1.13}] \rightarrow (MgO + NiO + MgAl_2O_4/NiAl_2O_4)$$

Magnesium containing hydrotalcite decomposition has been implemented via calcination at 650 °C and similar decomposition has been conducted by V. Rives and Ulibarri, 1999 [17]. Magnesium containing nano-crystalline mixed can be obtained at high pH (≥10) and the molar ratio of $M^{II}/M^{III} = 3$ [18]. Different calcination temperature other than 650 °C show less crystalline and bigger size of crystals [not shown here]. The XRD patterns of the mixed oxides indicate that the precursor of the synthesized materials had been decomposed fully, and characteristic hydrotalcite peaks disappeared from it at this temperature and led to the various oxide derivatives. The XRD analysis results compared with the JCPDS (joint committee of powder diffraction standard) references to assign the oxides and spinels of corresponding materials. The oxides and spinels have been symbolized with different symbols in Fig. 1. It is observed that Mg and Ni and Al containing mixed oxides are mainly oxides and spinel phases with the characteristic diffraction peaks of nickel aluminate; $NiAl_2O_4$ (JCPDS 10-0339), (MgNi)–O (JCPDS 1-77-396) and magnesium aluminates; $MgAl_2O_4$ (JCPDS-43–1022) in addition to the individual spinels: nickel oxides; NiO (JCPDS-22-1189) and magnesium oxides MgO (JCPDS-4–829). The situation of peaks overlapping is observed for MgO, NiO, $NiAl_2O_4$ and $MgAl_2O_4$ spinels. Some weak peaks of Al_2O_3 have been observed that are shown with overlapping of the peaks indicating that Al^{3+} cations are dispersed in the MgO structure without formation of spinel species. The formation of spinels MgAl2O4 and $NiAl_2O_4$ are due to the decrease of the activity of the hydrotalcite at high calcination temperature, and the basic sites are truly the hydroxyl groups rather than O^{2-} species [19].

It was found that calcination of Mg–Al HTlcs (MNAM 301) and Ni–Al HTlcs (MNAM 031) lead to finally MgO and $MgAl_2O_4$ and NiO and $NiAl_2O_4$ phases respectively [20,21]. Mg–Ni–Al HTlcs derived mixed oxides (MNAM 211, MNAM 121) show diffraction peaks overlapping at 2θ values of 37°,42.5°, 60° and 75° is due to the close (near) cationic radii of magnesium ($Mg^{2+} = 0.69$ Å) and nickel ($Ni^{2+} = 70$ Å) [in octahedral coordination) in the mixed oxides [22]. Meanwhile, the trivalent cations (Al^{3+}) disperse in the rock salt structure crystallite as AB_2O_4 spinels at high calcination temperature [23].

During hydrotalcite formation, Al^{3+} cations occupy the octahedral sites in hydrotalcite. Calcination at the high temperature, the structure of HTls rearranged and Al^{3+} cations substituted from octahedral to the tetrahedral site [24]. The generated positive charge in this replacement could be neutralized by the formation of cationic vacancies and/or inclusion of interstitial oxygens in the structure. A part of the tetrahedral aluminum locates at tetrahedral positions in MgO lattice which help to formation of the spinels. The O^{2-} ions adjacent to the magnesium (Mg^{2+}) and aluminum (Al^{3+}) become coordinative unsaturated and generate strong basic sites. The crystal size was measured using sheerer equation [16]. The average size of the crystal was 6–7 nm.

3.3. Morphologies of adsorbents

The FESEM image of MNAM 121 exhibits a porous microstructure (Fig. 2a) which can be ensured by BET nitrogen adsorption-desorption at −196 °C. The surface morphology of the mixed oxides depends on the synthesis condition (Temperature, pH) and chemical composition. The mixed oxides show two types of morphology which are the hexagonal plate-like [Fig. 2a] with an opening pore and the coral-like (MNAM 121) with a pore size of 80–100 nm and a slit-shape pore between two plates. The coral-like morphology (Fig. 2b) shows only when the pH of synthesis solution is 10. Porous materials with plate-like particles have geometry with openings between the plates. After calcination at the higher temperature the calcined hydrotalcite or mixed oxides still retained it shape of the crystal structure but increase it sizes which is due to the substitution of divalent cations (Mg^{2+}, Ni^{2+}) by trivalent cations of Al^{3+} in the burucite sheets and converted to periclase-like Mg–Al–O solid solution. Thus the burucite like shape of the crystal remained in resulting Mg/Ni–Al–O structure, which

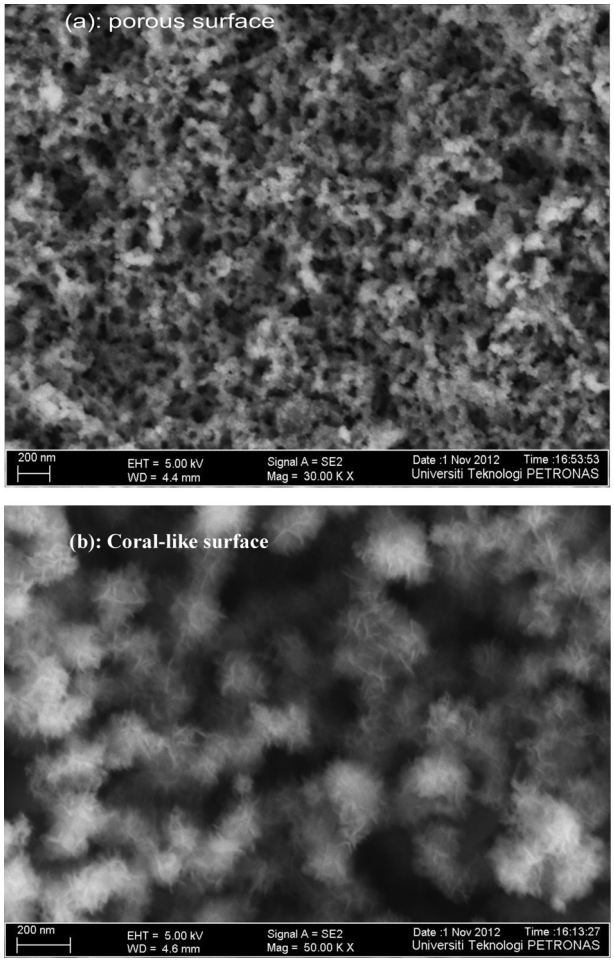

Fig. 2. FESEM Micrograph. (a) Porous surface of MNAM 121 (b) surface of MNAM 211 with coral like particle.

is in agreement with the work of W.T. Reichle et al., [25]. The formation of nano-crystalline hydrotalcite derived mixed oxides could be due to the nickel influence in the nucleation and crystal growth process during coprecipitation.

3.4. Microstructure analysis of adsorbent

The high resolution TEM image of MNAM 211 (Fig. 3) shows the average crystal size range of 6–8 nm and hexagonal plate-like crystal. Most of the investigated mixed oxide samples as appeared in the high resolution images were polycrystalline. The SAED pattern come from focused area (top corner of Fig. 3a) consisting of broad rings which is due to the presence of Mg_2NiO_4, MgO, NiO, $NiAl_2O_4$ and $MgAl_2O_4$ phases as indicated by their crystal planes that were confirmed by XRD results. Moreover, some additional weak, diffuse rings are due to the oxides of magnesium. From the observation, it has been realized that amorphous mixed oxides were unstable when expose electron beam for long time and appear in a weak crystalline form.

3.5. Microstructure of hydrogen adsorbed adsorbent

The diffused rings with bright spots in the SAED pattern (Fig. 3c) of hydrogen adsorbed crystal of MNAM 211 indicated the planes of (110), (202), (220), and (330). The planes are corresponding that the crystal is consisted with MgH_2, Mg_2NiH_4 and MgO [26]. The nano-

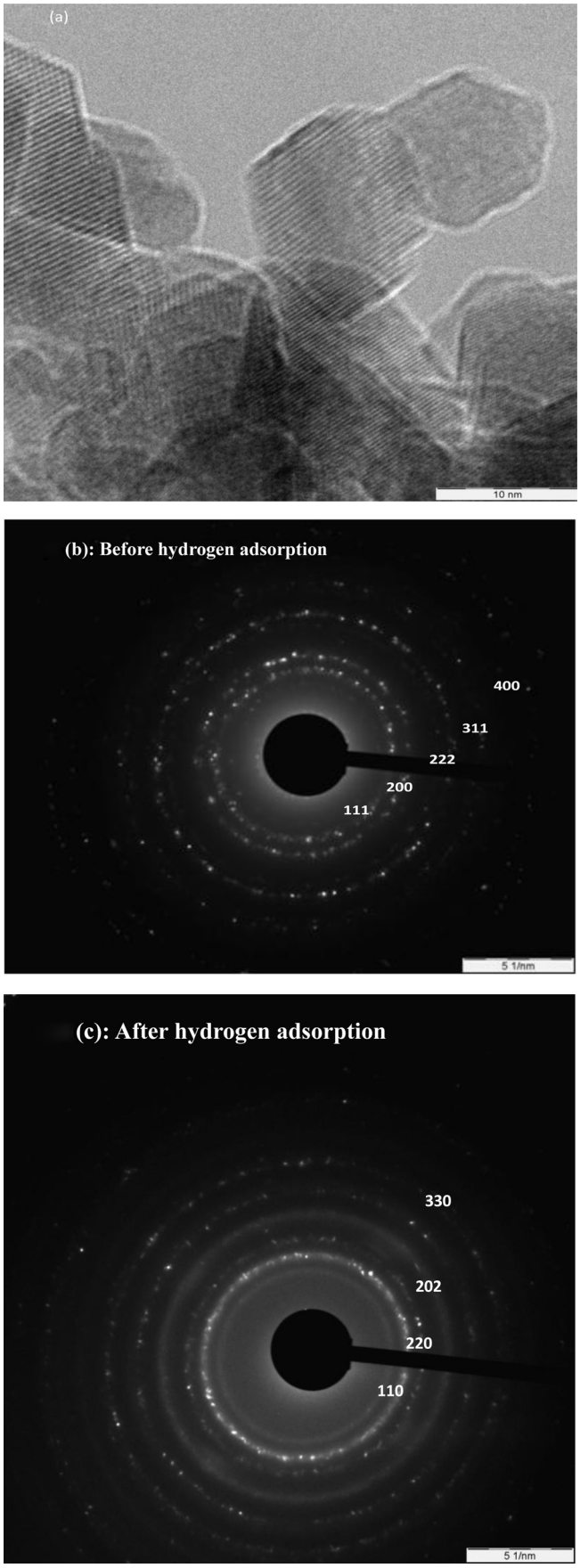

Fig. 3. TEM image of MNAM 211. (a) Hexagonal plate-like nano-crystal. (b) SAED pattern of crystal before H_2 adsorption. (c) SAED pattern of crystal after hydrogen adsorbed.

crystalline material has a well-established diffusion path for the hydrogen atom along the numerous grain boundaries and a slit shaped pore with opening geometry. In the case of nickel containing nano-crystalline mixed oxides, the nickel atoms may occupy meta-stable positions in the deformed grains that are caused by the change of the electronic structure of a valance band. So, the strong modifications of the electronic structure of nano-crystalline mixed oxides could effectively influence their hydrogenation behavior. The diffused rings with bright spot on the micrograph of the hydrogen adsorbed SAED pattern (Fig. 3c) are originate for hydrogen adsorbed compound that can be confirmed by the Raman and FTIR analyses. The major changes of the SAED pattern of crystal before and after the hydrogen adsorbed which is due to the chemisorption of the hydrogen on the reduced oxides surface that can be observed from Table 2 as well.

3.6. Textural properties of adsorbents

The isotherm of magnesium, nickel and aluminum containing (MNAM) mixed oxides (Fig. 4a) showed considerably sharp N_2 uptakes at high relative pressure and the presence of hysteresis loop indicated that mesoporosity generates due to the aggregation of the nano-particles [7]. Only magnesium containing mixed oxides showed hysteresis loop at high relative pressure near to unity. The completion of mesopores filling at high relative pressure values indicating that the mesopores were likely formed between platelets and capillary condensation was delayed. The hysteresis loops are vertical and parallel at high relative pressure which suggested the aggregates of plate-like particles leading to slit-shape pores of mixed oxides. The average pore diameters are above 13 nm indicating to interstices beyond 13 nm because of loose stacking mode.

Specific surface area of MNAM 211 and MNAM 121 are 325 and 284 $m^2\ g^{-1}$, respectively corresponding the formation of similar Mg(NiAl)O mixed oxide phases in both cases, whereas binary mixed oxides showed less specific surface area than ternary mixed oxides. Fornasari et al., also observed high specific surface area from Mg–Ni–Al ternary hydrotalcite derived mixed oxides [27]. The increased in surface areas upon slow calcination (temperature ramp 2 °C min^{-1} together with holding time (a) 2 h and allowed to cool down to room temperature) of hydrotalcite which is the cause of the formation of micro-and mesopores by removing CO_2, water and impurities from hydrotalcite.

The pore size distribution curve of MNAM showed a significant contribution of pores size ranges 5–13 nm and additionally a broad and varied contribution was also observed. The pore size distribution plot (Fig. 4b) showed narrow distribution for MNAM with peak pore width of 5–13 nm. The mixed oxides showed higher mesopores volume and the pore size distribution of MNAM 301 contains two peaks around 6 nm and 35 nm. The smaller pore distribution is corresponded to inter-crystalline distance within the aggregates whereas the large pore size distribution are likely originates from the inter-aggregate distances. The textural properties obtained from the BET analysis are summarized in Table 1.

Table 2
Hydrogen adsorption and desorption capacity of reduced mixed of MNAM

Adsorbent	Ads. capacity (mg g^{-1} adsorbent)	Des. capacity (mg g^{-1} adsorbent)
MNAM 031	20.40	4.98
MNAM 121	28.80	15.72
MNAM 211	38.69	18.95
MNAM 301	22.40	5.75

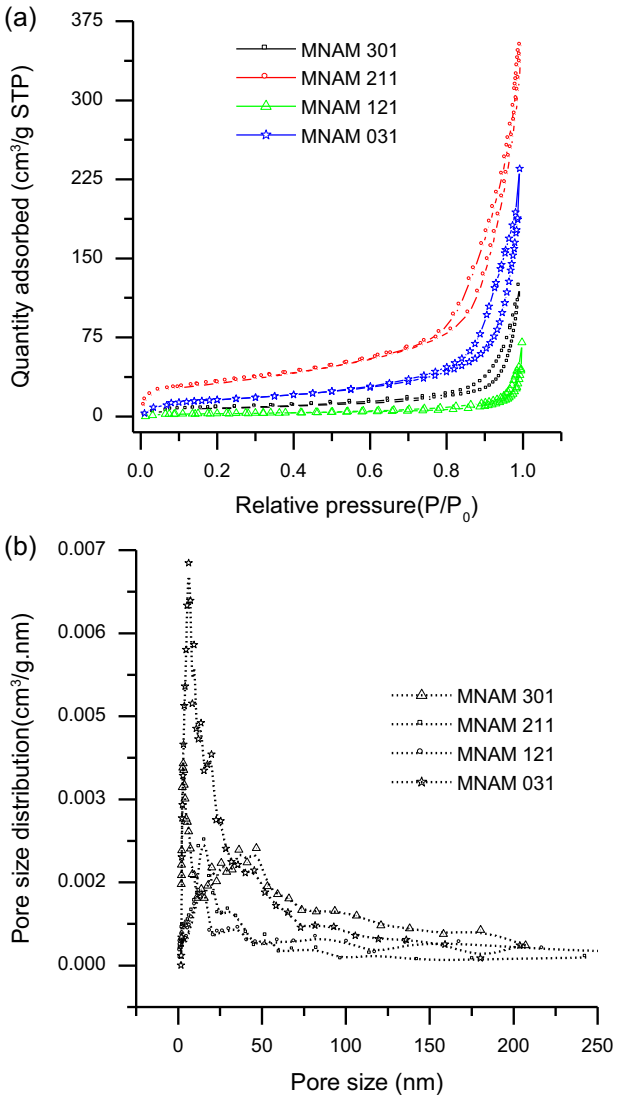

Fig. 4. (a) Isotherm curve of N_2 adsorption-desorption of MNAM. (b) PSD of MNAM with different molar ratios.

3.7. Hydrogen adsorption performance of mixed oxides

The hydrogen adsorption capacities of the Mg–Ni–Al reduced mixed oxides are shown in (Fig. 5). MNAM 031 or mixed oxides without magnesium show less hydrogen adsorption capacity whereas MNAM 301 or mixed oxides without nickel achieved higher capacity than that of MNAM031. The trend of the results is consistent with the stoichiometric capacity of magnesium and nickel. The significant phenomenon that can be observed is that ternary mixed oxides show higher hydrogen adsorption capacities than binary mixed oxides. MNAM 211 shows a 3.9 wt% hydrogen adsorption capacity (Table 2). Nickel works as a co-factors to improve kinetics, lower the binding energies of hydrogen on magnesium surface and reduces the migration barrier for the hydrogen, thus enhancing fast loading and uploading of hydrogen. The surface of reduced mixed oxides has a different lattice structure than a pure element structure (Mg) which is also an important factor to enhance the sorption of hydrogen. The dissociation of hydrogen molecules on the surface might occur with the help of nickel [28,29]. Magnesium with other light, main group elements such as aluminum (Al) lowers the affinity of hydrogen and competes with hydrogen for the valance electron of

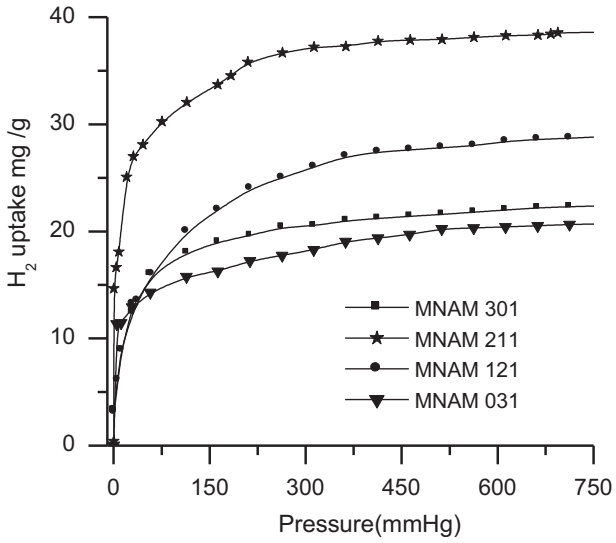

Fig. 5. Hydrogen adsorption capacity of reduced MNAM with different molar ratios at ambient conditions.

magnesium [30], and reduces the bonding strength between magnesium and hydrogen. Though nickel catalyses the magnesium to enhance the hydrogen adsorption, it reduces the weight percent of hydrogen in hydride. A mechanism can be considered for hydrogen adsorption on the basis of investigated chemical and structural properties. The dissociated hydrogen penetrates into magnesium and rapidly forms a layer of MgH_2 due to the negligible solid solubility of the hydrogen in the magnesium which also prevents the hydrogen from further diffusion. In the binary and ternary reduced mixed oxide, hydrogen may diffuse along boundaries between the Mg_2Ni and Mg_3Al_2 phases and also inside the Mg_2Ni phase. The hydrogen bonded with different phases of the magnesium compound and yields [31,32] are MgH_2 and Mg_2NiH_4 that can be confirmed through the characterization performed in this study:

$$Mg + nH = MgH_n$$

$$Mg_2Ni + nH = Mg_2NiH_n$$

3.8. Raman and FT-IR analysis of hydrogen adsorbed phases

The analyzed FT-IR and Raman spectra of hydrogen adsorbed MNAM 121 is shown in Fig. 6. The IR spectrum showed the three IR band at 450, 1000 and 1650 cm^{-1}. The bands at 450 and 1000 cm^{-1} are due to the formation of MgH_2 after adsorption of hydrogen [33,34]. And the band at 1650 cm^{-1} is attributed to the formation of Mg_2NiH_4 [35]. Raman spectrum of hydrogen adsorbed MNAM121 displayed several Raman shifts. Three Raman shifts at 313, 950 and 1270 cm^{-1} ensured the formation of the α-MgH_2 and the shifts are very consistent with the works of Santisteban et al., [34]. Again the Raman shifts with less intensity at 509, 707 cm^{-1} attributed the formation of γ-MgH_2 [36]. It is not clear the Raman shift at 1600 cm^{-1}. By comparing with the FT-IR, it can be considered that the shift is due to the Mg_2NiH_4 which indirectly implied by K Nakamoto [37].

3.9. Hydrogen decomposition

The H_2-TPD experiment was carried out at the temperature that was less than the reduction temperature to avoid an undesired thermal reaction. The H_2 desorption occurred in a wide

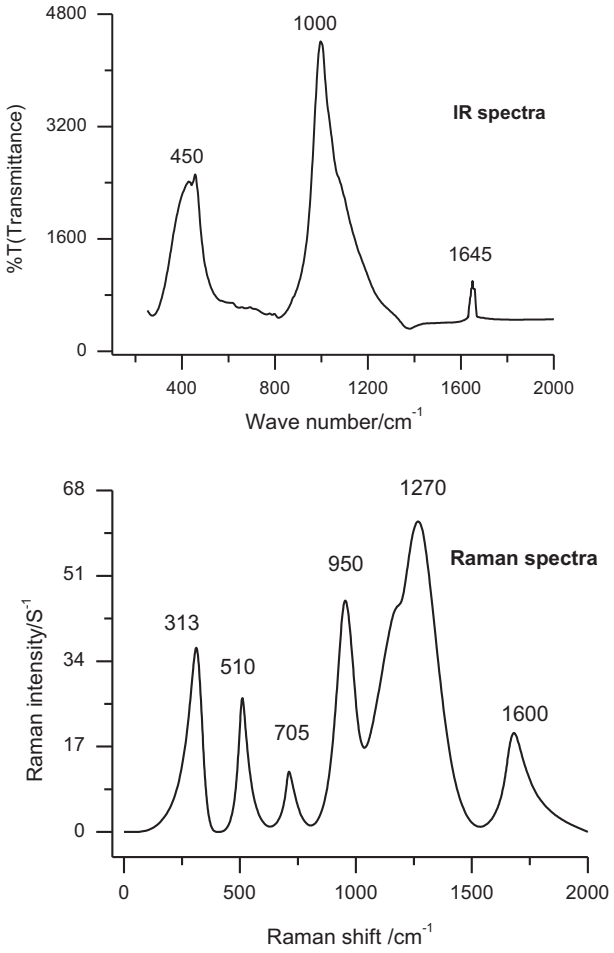

Fig. 6. FT-IR (top) and Raman (bottom) spectra of hydrogen adsorbed MNAM121.

temperature range and generally two peaks were noted for all profile (Fig. 7). The analysis revealed that a good amount of H_2 physisorbed on the surface of the mixed oxides at a temperature range of 50–120 °C and the rest of the chemisorbed H_2 desorbed at a higher temperature range. Hydrogen was not completely removed from the mixed oxides, which implies that incorporated H_2 is irreversibly chemisorbed in this solid (Table 2). The amount of the desorbed hydrogen was measured and quantified by a thermal conductivity detector (TCD). It can be observed that, without nickel; magnesium containing mixed oxides desorbed a less amount of hydrogen which might be a result of the strong binding of hydrogen with magnesium. The high temperature peak in the TPD profile of MNAM 211 was around 260 °C. It shows that a large amount of hydrogen desorbed at the temperature range of 250–350 °C. Hydrogen adsorbed phases of MgH_2 and Mg_2NiH_4 generally decompose at the temperature range of 240-400 °C and follow the decomposition reaction as mentioned below [38]

$$Mg_2NiH_4 \rightarrow Mg_2Ni + 2H_2 \quad (240\ ^\circ C)$$

$$MgH_2 \rightarrow Mg + H_2 \quad (395\ ^\circ C)$$

Therefore, the maximum hydrogen was desorbed from the mentioned hydrogen adsorbed phases. The metal-support interaction shows an important role. During desorption, hydrogen atoms on the support would migrate back to the metal surface and recombine with hydrogen molecules then desorb from the surface due to the hydrogen spillover between them. It is thought that the electronic property of Ni^0 changes more rigorously with increasing

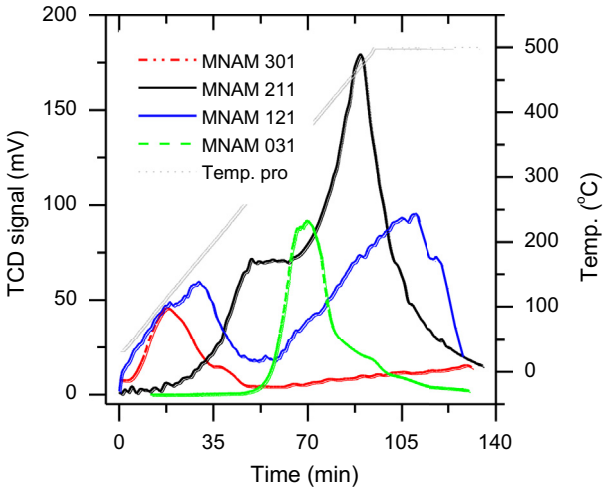

Fig. 7. H_2-TPD of mixed oxides of MNAM with different molar ratios.

the molar content of Mg and Ni [39] which enhance the adsorption and desorption process.

4. Conclusion

The mixed oxides have been characterized using different techniques to investigate physio-chemical properties of hydrotalcite based mixed oxides as hydrogen adsorbent at ambient conditions. Adsorption and desorption process at the ambient temperature (30 °C) and pressure (760 mmHg) were enhanced via the catalytic effect of specific concentration of nickel. The concentration ratio of nickel with magnesium, 2:1 is the best combination to catalyze the magnesium for hydrogen uptake. Nano-structured polycrystalline reduced mixed oxides of MNAM 211 showed a 3.9 wt% hydrogen adsorption capacity. The co-existence of aluminum and nickel could modify the electronic structure of the mixed oxides surface and the dissociated reactive hydrogen species diffused and bind from bulk to different transitional phases that desorbed at 395 °C. Raman and FTIR analysis confirmed the hydrogen adsorbed phase of MgH_2 and Mg_2NiH_4. The material can be used to different industrial application as energy storage materials.

Acknowledgements

We would like to acknowledge gratefully the financial support of this research by the FRGS grant 158-200-092, Malaysia.

References

[1] J.J. Vajo, G.L. Olson, Scripta Mater. 56 (2007) 829.
[2] B. Bogdanovic, J.H. Hartwig, B. Spliethoff, Int. J. Hydrogen Energy 18 (1993) 575.
[3] A. Borgschulte, R.J. Westerwaal, J.H. Rector, H. Schreuders, B. Dam, R. Griessen, J. Catal. 239 (2006) 263.
[4] A. Zaluska, L. Zaluski, J.O. Stroem-Olsen, J. Alloys Comp. 289 (1999) 197.
[5] C.O. Arean, S. Chavan, C.P. Cabello, E. Garrone, G.T. Palomino, ChemPhysChem 11 (2010) 3237.
[6] M.K. Thomas, Catal. Today 20 (2007) 389.
[7] M.A. Salam, S. Sufian, Y. Lwin, T. Murugesan, Nanomaterials 2013 (2013) 1.
[8] P.B.D. Cornelis, P.C.H. Bart, H.B.D. Johannes, P.J. Krijn, Chem. Int. Ed. 45 (2006) 3501.
[9] M.A. Salam, S. Suriati, Y. Lwin, J. Phys. Chem. Solids 74 (2013) 558.
[10] F. Bergaya, B.K.G. Theng, G. Lagaly, Handbook of Clay Science, vol. 1, Elsevier, Amsterdam, 2006, 1224.
[11] B. Shouli, L. Dianqinga, H. Dongmei, L. Ruixian, C. Liu, C. Aifan, Sens. Actuat. B150 (2010) 749.
[12] K. Zakrzewska, Thin Sol. Films 391 (2001) 229.
[13] D.L. Jalowiecki, S. Debeusscher, H. Zarrou, A. D'Huysser, H. Jobic, E. Payen, Catal. Today 138 (2008) 266.
[14] H.S. Kim, C. Kwang-Seo, B.K. Yoo, T.G. Ryu, Y.S. Lee, C.S. Park, Y.H. Kim, J. Ind. Eng. Chem. 16 (2010) 81.
[15] C. Lucjan, K. Piotr, R. Alicja, D. Roman, Thermochimica Acta 395 (2003) 225.
[16] M.A. Salam, Y. Lwin, S. Suriati, Adv. Mat. Res. 626 (2013) 173.
[17] V. Rives, M.A. Ulibarri, Coord. Chem. Rev. 181 (1999) 61.
[18] U. Olsbye, D. Akporiaye, E. Rytter, M. Rønnekleiv, E. Tangstad, Appl. Catal. A Gen. 224 (2002) 39.
[19] T. Didier, H.L. Mohammed, G. Alain, H.C. Bich, F. Francois, A. Aline, B. Davide, G. Edoardo, J. Catal. 151 (1995) 50.
[20] F.M. Labajos, V. Rives, M.A. Ulibarri, J. Mater. Sci. 27 (1992) 1546.
[21] O.W. Perez-Lopez, A. Senger, N.R. Marcilio, M.A. Lansarin, Appl. Catal. A Gen. 303 (2006) 234.
[22] J.A. Rivera, G. Fetter, Y. Jiménez, M.M. Xochipa, P. Bosch, Appl. Catal. A Gen. 316 (2007) 207.
[23] M.J. Holgado, V. Rives, M.S. San Román, Appl. Catal. A Gen. 214 (2001) 219.
[24] A. Corma, V. Fornes, F. Rey, J. Catal. 148 (1994) 205.
[25] W.T. Reichle, S.Y. Kang, D.S. Everhardt, J. Catal. 101 (1986) 352.
[26] J. Zou, H. Sun, X. Zeng, G. Ji, W. Ding, J. Nanomaterials 2012 (2012) 1.
[27] G. Fornasari, M. Gazzano, D. Matteuzzi, F. Trifir, A. Vaccari, Appl. Clay Sci. 10 (1995) 69.
[28] Y. Fukai, The Metal-hydrogen System – Basic Bulk Properties, Springer-Verlag, Berlin, 1993.
[29] N. Huang, H. Yamauchi, J. Wu, Q.Z. Wang, Phys. Chem. Munich 163 (1989) 225.
[30] J. Topler, H. Buchner, H.S. Aufferer, K. Knorr, W. Prandl, Less. Comm. Met 88 (1982) 397.
[31] G. Duarte, L.A.C. Bustamante, P.E.V. Miranda, WHEC 16 (2006) 13.
[32] S. Billur, L.D. Farida, H. Michael, Int. J. Hydrogen Energy 32 (2007) 1121.
[33] H. Hiroshi, Quantitative Evaluation of Catalytic Effect on the Desorption Reaction of Hydrogen Storage Materials on the Basis of Atomization Energy Concept, PhD thesis, Nagoya University, 2010.
[34] J.R. Santisteban, G.J. Cuello, J. Davidowski, A. Fainstein, H.A. Peretti, A. . Ivanov, F.J. Bermejo, Phys. Rev. B 62 (2000) 37.
[35] L.J. Huang, G.Y. Liang, Z.B. Sun, D.C. Wu, J. Power Sources 160 (2006) 684.
[36] T. Moriwaki, Y. Akahama, H. Kawamura, S. Nakano, K. Takemura, J. Phys. Soc. Jpn. 75 (7) (2006) 074603.
[37] K. Nakamoto, Infrared and Raman Spectra of Inorganic and Coordination Compounds, fourth ed., Wiley, New York, 1986, p. 130.
[38] J. Zou, H. Sun, X. Zeng, G. Ji, J. Nanomaterials 2012 (2012) 1.
[39] P. Kim, Y. Kim, H. Kim, I.K. Song, J. Yi, J. Mol. Catal. A Chem. 231 (2005) 247.